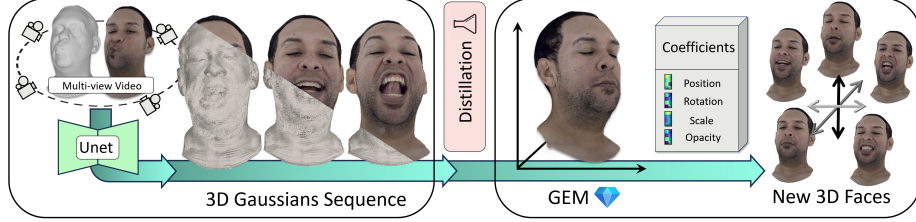


# Gaussian Eigen Models for Human Heads

Wojciech Zielonka<sup>1</sup>, Timo Bolkart<sup>2</sup>, Thabo Beeler<sup>2</sup>, and Justus Thies<sup>1,3</sup>

<sup>1</sup>Max Planck Institute for Intelligent Systems, Tübingen, <sup>2</sup>Google, <sup>3</sup>TU Darmstadt  
<https://zielon.github.io/gem/>



**Fig. 1:** Given a multi-view video of a subject and meshes in full correspondence, we construct a high-quality Gaussian Eigen Model (GEM). Our method, employing a UNet (left), regresses a sequence of 3D Gaussians that undergo distillation to obtain compressed linear eigenbasis which we call Eigen Gaussians (right). To generate new photo-realistic 3D faces only a linear combination of the Gaussian basis has to be computed. We show that the required coefficients for the linear combination can be regressed from single images, allowing for real-time facial animation. The simplicity of a GEM leads to very efficient storage and rendering times.

**Abstract.** We present personalized Gaussian Eigen Models (GEMs) for human heads, a novel method that compresses dynamic 3D Gaussians into low-dimensional linear spaces. Our approach is inspired by the seminal work of Blanz and Vetter, where a mesh-based 3D morphable model (3DMM) is constructed from registered meshes. Based on dynamic 3D Gaussians, we create a lower-dimensional representation of primitives that applies to most 3DGS head avatars. Specifically, we propose a universal method to distill the appearance of a mesh-controlled UNet Gaussian avatar using an ensemble of linear eigenbasis. We replace heavy CNN-based architectures with a single linear layer improving speed and enabling a range of real-time downstream applications. To create a particular facial expression, one simply needs to perform a dot product between the eigen coefficients and the distilled basis. This efficient method removes the requirement for an input mesh during testing, enhancing simplicity and speed in expression generation. This process is highly efficient and supports real-time rendering on everyday devices, leveraging the effectiveness of standard Gaussian Splatting. In addition, we demonstrate how the GEM can be controlled using a ResNet-based regression architecture. We show and compare self-reenactment and cross-person reenactment to state-of-the-art 3D avatar methods, demonstrating higher quality and better control. A real-time demo showcases the applicability of the GEM representation.

**Keywords:** Eigen Head Avatars, Gaussian Splatting

## 1 Introduction

Half a century ago, Frederick Parke described a representation and animation technique to generate „animated sequences of a human face changing expressions” [48]. Using polygonal meshes, single facial expression states were described that could be combined with linear interpolation to generate new expression states (the „simplest way consistent with natural motion” [48]). Based on this principle, Blanz, and Vetter [3] introduced the so-called 3D morphable model (3DMM) - a statistical model of the 3D shape and appearance of human faces. Principle Component Analysis (PCA) is performed on a set of around 200 subjects that have been laser scanned and registered to a consistent template to find the displacement vectors (principal components) of how faces change the most, in terms of geometry and albedo. With this PCA basis, new faces can be generated by specifying the coefficients for the principle components taking a dot product of the coefficients with the basis to obtain offsets, and adding them to the mean. State-of-the-art reports on face reconstruction and tracking [86], as well as on morphable models [8], state that this representation is widely used for performance capturing (regression-based and optimization-based) and builds the backbone of recent controllable photo-realistic 3D avatars that are equipped with neural rendering [11, 17, 63, 64, 81].

Inspired by the simplicity of such mesh-based linear morphable models and addressing the lack of appearance realism of current 3DMMs, we propose a personalized linear appearance model based on 3D Gaussians as geometry primitive following 3D Gaussian Splatting (3DGS) [28]. In contrast to the concurrent work on Dynamic 3D Gaussian Avatars [38, 47, 53, 59, 74, 79, 83], our goal is a compact representation that does not need vast amounts of compute resources to generate novel expressions of the human. Unfortunately, most of the methods show that to produce high-quality results, one needs to employ heavy CNN-based architectures which are not well suited for commodity devices and tend to slow down the rendering pipeline. Moreover, those models comprise dozens of millions of parameters creating heavy checkpoints that can easily exceed 500 MB. This ultimately creates a major issue for distributing and managing personalized models. We tackle this problem by distilling a novel CNN-based architecture, leading to a personalized **Gaussian Eigen Model**, **GEM** in short. Our approach builds on Gaussian maps predicted from a modified UNet architecture [69] which is used for the UV space normalization required to properly build linear eigenbasis. Based on the per-subject trained model, we bootstrap the personalized GEM by computing an ensemble of linear basis on the predicted Gaussian maps of the training frames. Next, the basis is refined on the training corpus using photometric losses while preserving the orthonormality.

This lightweight appearance basis is controlled with a relatively low number of parameters ranging from twenty up to fifty coefficients which can be specified w.r.t. the available compute resources and can for example be regressed by a ResNet-based model [9]. We demonstrate this for the scenarios of self-reenactment as well as cross-person animation. We showcase a real-time application of our method in the supplemental video.



In summary, our contributions are:

1. Gaussian Eigen Model (GEM) a universal distillation technique of 3D Gaussian head avatar model that is built upon an ensemble of eigenbasis.
2. A state-of-the-art CNN-based avatar appearance model that can be constructed using multi-view captures of a subject and serves as an example that can be used in combination with GEM.
3. Real-time (cross-person) animation of GEMs from single input images using a generalizable regressor.

## 2 Related Work

The majority of current face representations and tracking techniques are based on parametric 3D morphable models (3DMM) [3, 37]. For a detailed overview of 3DMM-based reconstruction and appearance models, we refer to the state-of-the-art reports on face tracking and reconstruction [86], the report on morphable models [8], and the two neural rendering state-of-the-art reports [63, 64] that demonstrate how neural rendering can be leveraged for photo-realistic facial or full body avatars. In the following, we review the recent methods that are focused on photo-realistic 3D avatars which build appearance models using neural radiance fields (NeRF) [43] or volumetric primitives like 3D Gaussians [28].

### 2.1 NeRF-based avatars

One of the first methods that combined 3DMM and NeRF is NeRFace [11]. In this work, a neural radiance field is directly conditioned by expression codes using the Basel Face Model (BFM) [3] optimized by the Face2Face tracker [67]. This idea gave rise to many methods [12, 17, 52, 76, 78, 81, 82, 84] following a similar approach, but attaching the radiance fields more explicitly to the surface of the 3DMM, e.g., by using the 3DMM-defined deformation field. To enable photorealistic results some methods employ StyleGAN2 [27] with a NeRF-based renderer [1, 5, 26]. Generative methods like EG3D [5] and PanoHead [1] employ a GAN-based training to predict triplane features that span a neural radiance field. GANAvatar [26] applies this scheme to reconstruct a personalized avatar.

Close to our method is StyleAvatar [69]. Based on 3DMM tracking the method learns a personalized avatar that benefits from a StyleUNet which incorporates StyleGAN [27] to decode the final image. Despite real-time capabilities, the method suffers from artifacts produced by the image-to-image translation network that we explicitly avoid by using Gaussian maps which can compensate for tracking misalignments by predicting corrective fields for the 3D Gaussians.

### 2.2 3D Avatars from Volumetric Primitives

Neural Volumes (NV) [39] started an impressive line of research in the context of digital avatars. Using multiview images with a Variational Auto-Encoder [30]

and volumetric integration it encodes arbitrary dynamic scenes into a volume which can be deformed by traversing the latent code  $\mathbf{z}$ . To better control the 3D space, Lombardi et al. [40] introduced Mixture of Volumetric Primitives (MVP) a hybrid representation based on primitives attached to the tracked mesh which ultimately replaced the encoder from NV. Each primitive is a volume represented as a small voxel with  $32^3$  cells that on the vertices store RGB and opacity values. The final color is obtained by integrating values along a pixel ray. This hybrid representation became very popular spawning many follow-up projects [4, 36, 55, 62, 71]. The recently presented 3D Gaussians Splatting (3DGS) [28] introduced an alternative representation to MVP primitives. 3DGS represents a volume as a set of anisotropic 3D Gaussians, which are equivalently described as ellipsoids, in contrast to isotropic spheres used in Pulsar [35]. Similarly to DSS [70] it defines a backward pass of the rasterization technique Surface Splatting introduced by Zwicker et al. [87]. However, with the difference of using  $\alpha$ -blending [43] to integrate 3D Gaussians along a given ray. Numerous recent methods [10, 15, 24, 32, 38, 47, 53, 59, 73, 74, 80, 83] capitalize on the speed and quality of 3DGS. Qian et al. attached 3D Gaussians to the FLAME [37] mesh surface and applied a deformation gradient similar to Zielonka et al. [84] to orient the Gaussians according to the local Frenet frames of the surface. This method, however, does not utilize any information about expressions and, thus, struggles with pose-dependent changes (e.g., wrinkles, self-shadows) and, despite high-quality results, retrieves only a global static appearance model. Li et al. [38] are using the StyleUNet architecture [69] to regress front and back Gaussian maps. Employing the powerful CNN network on position maps, they achieve impressive results for human bodies. However, their architecture uses three separate StyleUNets each with two decoders for front and back texture which creates significant computational overhead making the whole pipeline slow. In contrast, we propose a more efficient CNN-based model that operates in a UV-space which we distill a lightweight linear 3D Gaussian Eigen Model (GEM).

### 3 Method

Current dynamic 3D Gaussian Avatars show unprecedented quality, however, they require sophisticated and often compute-heavy CNN-based architectures [38, 47, 74] leveraging large receptive fields to capture high-frequency details like pose-dependent wrinkles or self-shadows. We present an efficient CNN-based high-quality model and propose a technique to compress and distill such an avatar into an ensemble of eigenbasis that preserves its neural counterpart’s quality and expressiveness. The following section will explain our novel CNN-based appearance model and how to distill it into an alternative representation called the Gaussian Eigen Model (GEM).

*Note that compared to other neural avatars [11, 17, 39, 69, 74, 84], GEM does not require a 3DMM [37, 50], i.e., training GEM only requires meshes in correspondence, while testing uses the GEM model parameters, making it effectively mesh and neural network free.*

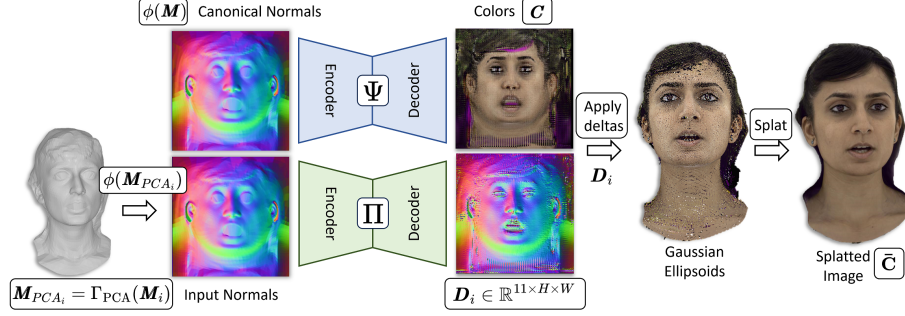


**Fig. 2: CNN-based Gaussian Avatar Pipeline.** Our CNN model produces delta Gaussian maps  $D_i$  [38, 47] and static color  $C$  from a multi-view video. Similarly to Animatable Gaussians [38], we constrain the network to operate in a reduced linear space, i.e., the mesh  $M_i$  is projected on a PCA basis  $M_{PCA_i} = \Gamma_{PCA}(M_i)$  which is then input to the network  $\Pi$  after converting the mesh to a normal map  $\phi(M_{PCA_i})$ .

### 3.1 3D Gaussian Splatting Preliminaries

3D Gaussian Splatting (3DGS) [28] is an alternative approach to Neural Radiance Field (NeRF) [43] for static multi-view scene reconstruction and rendering under novel view. Kerbl et al. [28] parameterize the space as scaled 3D Gaussians [34, 70] with a 3D covariance matrix  $\Sigma$  and mean  $\mu$ :

$$G(\mathbf{x}) = e^{-\frac{1}{2}(\mathbf{x}-\mu)^T \Sigma^{-1}(\mathbf{x}-\mu)}. \quad (1)$$

To render this representation, Zwicker et al. [87] employ the projection of 3D Gaussians onto the image plane using the formula  $\Sigma' = \mathbf{A}\mathbf{W}\Sigma\mathbf{W}^T\mathbf{A}^T$ , where  $\Sigma'$  represents the covariance matrix in 2D space. Here,  $\mathbf{W}$  denotes the view transformation, and  $\mathbf{A}$  represents the projective transformation. To avoid direct optimization of the covariance matrix  $\Sigma$  which must be positive semidefinite, Kerbl et al. [28] use scale  $\mathbf{S}$  and rotation  $\mathbf{R}$  which equivalently describes 3D Gaussian as a 3D ellipsoid  $\Sigma = \mathbf{R}\mathbf{S}\mathbf{S}^T\mathbf{R}^T$ . Finally, 3DGS follows Ramamoorthi et al. [54] to approximate the diffuse part of the BRDF [16] as spherical harmonics (SH) to model global illumination and view-dependent color. Four bands of SH are used which results in a 48 elements vector.

### 3.2 Appearance Maps Generator

As an example of a powerful Gaussian generator, we present a CNN-based appearance model inspired by Pix2Pix [22], which translates an input image to a specific output domain. In our case, Gaussian maps are generated from coarse normal maps of a tracked mesh. The idea of organizing the 3D Gaussians in 2D maps is used in several methods [38, 47, 74]; each texel in such a map represents a 3D Gaussian with its parameters: offset vector for rotation, scale, position, and opacity. Similarly to StyleAvatar [69], we use a StyleGAN-based [27] encoder and decoder network for this image translation. However, in contrast to StyleAvatar, we propose a more lightweight image translation pipeline, where we reduce the

number of encoders from three to two and the number of decoders from six to two, and decrease the size of the StyleGAN [27] decoder. To efficiently use the 2D map space, we do not use projective textures from meshes [69], but a UV parametrization which reduces half of the decoders in comparison to StyleAvatar. Moreover, we do not use triplets of the encoder-decoder, as we combine all properties of the Gaussians into one map  $\mathbf{G}_i$  following ASH [47]. Therefore, we define our network as follows:

$$\begin{aligned}\mathbf{D}_i &: \Pi(\phi(\Gamma_{\text{PCA}}(\mathbf{M}_i))), \\ \mathbf{C} &: \Psi(\phi(\mathbf{M})),\end{aligned}\tag{2}$$

where  $\mathbf{D}_i \in \mathbb{R}^{11 \times H \times W}$  is a map containing the delta for positions  $\Delta_{pos} \in \mathbb{R}^3$ , rotation  $\Delta_{rot} \in \mathbb{R}^4$ , scale  $\Delta_{scale} \in \mathbb{R}^3$ , and opacity  $\Delta_{op} \in \mathbb{R}$ . The colors  $\mathbf{C} \in \mathbb{R}^{3 \times H \times W}$  of the Gaussians are predicted using the normal map  $\phi(\mathbf{M})$  of the canonical mesh  $\mathbf{M}$  ( $\phi$  is the normal map extractor from a mesh). Similar to Animatable Gaussians [38], we use a PCA layer  $\Gamma_{\text{PCA}}$  which serves as a low-pass regularization filter for the input.  $\Gamma_{\text{PCA}}$  is built by using PCA on the meshes  $\mathbf{M}_i$  for the training frames and 16 principle components are used as the basis. For the training, we use the projection of each incoming mesh  $\mathbf{M}_i$  on the PCA manifold  $\mathbf{M}_{PCA_i} = \Gamma_{\text{PCA}}(\mathbf{M}_i)$ .

The final Gaussian map  $\mathbf{G}_i \in \mathbb{R}^{11 \times H \times W}$  is obtained by applying the deltas to the canonical Gaussians  $\mathbf{G}$  [38, 83]. The deformed position of 3D means is computed as  $\mathbf{T}_i(\mathbf{M} + \mathbf{D}_{i0:3})$  (Section 3.3). Note that our color map  $\mathbf{C}$  is static and does not model view-dependent effects; this means that we force the network to recover globally consistent colors for each Gaussian similar to a texture in the classic 3DMM. Therefore,  $\mathbf{G}_i$  must model the wrinkles and self-shadows.

Finally, we use Gaussian splatting [28] to render the regressed Gaussian maps. We define the predicted color of pixel  $(u, v)$  as:

$$\bar{\mathbf{C}}_{u,v} = \sum_{i \in \mathcal{N}} \mathbf{c}_i \alpha_i \prod_{j=1}^{i-1} (1 - \alpha_j),\tag{3}$$

where  $\mathbf{c}_i$  is the Gaussian color predicted by  $\Psi$ ,  $\mathcal{N}$  is the number of texels and  $\alpha_i$  is predicted opacity per Gaussian.

### 3.3 Deformation Model

The output of the CNN regressors  $\Pi$  and  $\Psi$  are in a canonical space. For the transformation from the canonical space to the deformed space, we employ deformation gradients, following Sumner et al. [60]. This approach allows for greater flexibility regarding input meshes, provided they maintain full correspondence. Given a mesh  $\mathbf{M}_{PCA_i}$  for the frame  $i$ , we define the deformation gradients as  $\mathbf{J}_j = \dot{\mathbf{E}}_j \mathbf{E}_j^{-1}$ , where  $\dot{\mathbf{E}}_j \in \mathbb{R}^{3 \times 3}$  and  $\mathbf{E}_j \in \mathbb{R}^{3 \times 3}$  contain the Frenet frame (tangent, bi-tangent, normal) of the triangle  $j$  defined in deformed and canonical spaces, respectively. Using these deformation gradients and the known correspondences between the Gaussian map and the meshes, we transform the Gaussians from the canonical space to the deformed space.

### 3.4 Implementation Details

The training objective of the CNN-based appearance model is defined as  $\mathcal{L} = \mathcal{L}_{Color} + \mathcal{L}_{Reg}$ .  $\mathcal{L}_{Color}$  is a weighted sum of three different photo-metric losses between the rendered image  $\tilde{\mathbf{C}}$  and the ground truth  $\mathbf{C}$ :

$$\begin{aligned}\mathcal{L}_{Color} &= (1 - \omega)\mathcal{L}_1 + \omega\mathcal{L}_{D-SSIM} + \zeta\mathcal{L}_{VGG}, \\ \mathcal{L}_{Reg} &= \lambda \sum_{j=1}^N \|\Delta_{pos_j}\|^2 + \gamma \sum_{j=1}^N \|s_{scale_j}\|^2,\end{aligned}\tag{4}$$

where  $\omega = 0.2$ ,  $\zeta = 0.0075$  (after 150k iterations steps and zero otherwise),  $\mathcal{L}_{D-SSIM}$  is a structural dissimilarity loss, and  $\mathcal{L}_{VGG}$  is the perceptual VGG loss.  $\mathcal{L}_{Reg}$  regularizes position offsets  $\Delta_{pos_j}$  and scales  $s_{scale_j}$  to stay small w.r.t. the input mesh. We train our model for  $10^6$  steps using Adam [29] with a learning rate  $5e-4$  and a batch size of one which takes around 24h on a Nvidia A100.

Our method and all the baselines were trained using the same multiview input data sourced from the dataset provided by Qian [53], which includes multiview images from the NeRSamble dataset [33] as well as tracked meshes. These datasets are licensed and managed by MPI and TuD.

## 4 Gaussian Eigen Model (GEM)

Once a powerful appearance generator is available, we can build our universal eigenbasis model, GEM. For each training frame, we save the predicted Gaussian maps  $\mathbf{G}_i$ , where the positions are normalized by un-posing the head joint. The Gaussian maps could be successfully replaced with Gaussian point clouds, as long as their quantity remains unchanged. We stack the Gaussian maps in a matrix  $\mathbf{A} \in \mathbb{R}^{N \times 11 \times H \times W}$  where  $N$  is the number of frames. Since the color  $\mathbf{C}$  was optimized globally, it acts like a classic texture and therefore does not need distillation. We build our statistical model for each modality of the Gaussians



**Fig. 3: Samples of a GEM.** We display samples for the first three components of the geometry eigenbasis of a GEM in the range of  $[-3\sigma, 3\sigma]$ , showing diverse expressions. Note that GEM requires **no** parametric 3D face model like FLAME [37].

from  $\mathbf{A}$  separately, specifically, we have individual bases for rotation, position, opacity, and scales. To compute the ensemble of eigenbasis we use Scikit-learn

[51] and PCA [25] and define our model as an orthogonal coordinate system formed by the eigenvectors of the covariance matrices of each modality, formally we solve:

$$(\mathbf{A}^T \mathbf{A}) \mathbf{V} = \mathbf{V} \mathbf{\Lambda}, \quad (5)$$

where  $\mathbf{A}^T \mathbf{A} \in \mathbb{R}^{M \times M}$  is the covariance matrix,  $\mathbf{V} \in \mathbb{R}^{M \times M}$  is the matrix of eigenvectors and  $\mathbf{\Lambda} \in \mathbb{R}^{M \times M}$  is the diagonal matrix of eigenvalues ( $M = N \times 11 \times H \times W$ ). Thus, per modality, we have:

$$\mathbf{S}_{mod} = \bar{\mathbf{S}}_{mod} + \sum_{i=1}^m \lambda_i \mathbf{v}_i, \quad (6)$$

where  $\lambda_i$  are coefficient ( $\mathbf{\Lambda}_{:,i}$ ),  $\bar{\mathbf{S}}_{mod}$  is a given modality mean,  $\mathbf{v}_i$  are the spanning vectors of the corresponding orthonormal basis  $\mathbf{V}_{:,i}$ , and the number of principal components is set to  $m = 50$ . 3 depicts samples of a GEM on the 3D position modality. For the remainder of the document, we omit the *mod* index for simplicity.

After estimating the initial basis  $\mathbf{V}$  which might contain artifacts produced by the CNN network, we refine it using a photometric reconstruction loss on the training images for around 30k iterations employing the same objectives from Equation 4 to obtain  $\hat{\mathbf{V}}$ . To ensure that the basis stays orthonormal throughout this refinement, every 1k steps, we orthogonalize  $\hat{\mathbf{V}}$  using QR decomposition such that  $\hat{\mathbf{V}}^T \hat{\mathbf{V}} = \hat{\mathbf{V}} \hat{\mathbf{V}}^T = \mathbf{I}$ . Example training PSNR errors w.r.t refinement steps 0k, 5k, and 30k are 34.75dB, 36.68dB, and 36.85dB, respectively, showing further improvement in the quality.

#### 4.1 Image-based animation of GEM

Expressions for a GEM are fully defined by their coefficients. This is a similar idea to codec avatars introduced by Ma et al. [42], however, our approach does not need additional small regression MLPs. There are several ways to obtain the coefficients of a GEM, for example, one could employ analysis-by-synthesis-based optimization or regression. Analysis-by-synthesis is the backbone of current avatar methods, as they use photometric or depth-based face trackers to sequentially optimize the coefficients of the underlying 3DMMs like FLAME [17, 67, 84] which is typically slow. As a fast, but more imprecise alternative, regressors like DECA [9] or EMOCA [7] can be used which are built on a ResNet backbone and regress FLAME parameters directly from an image.

As we aim for fast and expressive motion capturing, we build a personalized GEM regressor, that builds upon EMOCA, however, with several major modifications, see 4. First, we do not use FLAME parameters, instead, we use features extracted from a pre-trained EMOCA network denoted as  $\Theta(\mathbf{I}_i)$  where  $\mathbf{I}_i$  is the current image. EMOCA’s architecture comprises two ResNet networks; one to extract expression features  $\mathbf{f}_{expr} \in \mathbb{R}^{2048}$  and the second for shape  $\mathbf{f}_{shape} \in \mathbb{R}^{2048}$ , both are followed by final MLPs to regress corresponding FLAME parameters. In contrast, we remove the last hidden layer of the final MLP obtaining features



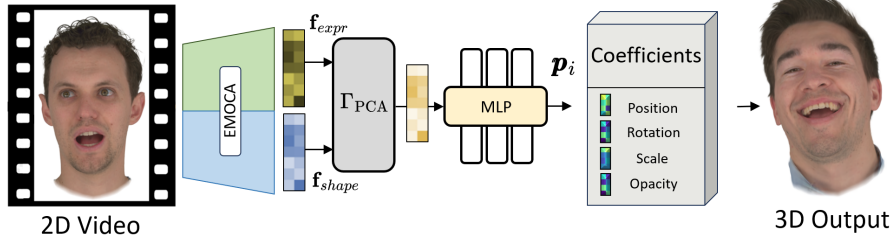


**Fig. 4: Image-based animation.** One of the applications of our GEM is real-time (cross)-reenactment. For that, we utilize generalized features from EMOCA [7] and build a pipeline to regress the PCA coefficients of our model from an input image/video.

$\in \mathbb{R}^{1024}$  and combine the regressed vectors into one  $\mathbf{f}_i \in \mathbb{R}^{2 \times 1024}$  vector. For training, we select five frontal cameras from NeRSemble [33]. Next, we build a PCA layer using the training frames similar to the one from our appearance model, however, with the difference that we use relative features  $\mathbf{r}_i = \mathbf{f}_i - \mathbf{f}_{neutral}$  instead of meshes. The neutral reference frame  $\mathbf{f}_{neutral} = \Theta(\mathbf{I}_{neutral})$  is selected manually from the video similar to Face2Face [67]. During training, for each frame, we project  $\mathbf{r}_i$  onto the PCA manifold to restrict and regularize training using the first 50 components. The projected coefficients are passed through a small MLP that produces a vector of GEM coefficients per modality, denoted as  $\mathbf{p}_i \in \mathbb{R}^M$ :

$$\begin{aligned} \mathbf{r}_i &= \Theta(\mathbf{I}_i) - \mathbf{f}_{neutral}, \\ \mathbf{p}_i &= 3\sigma \cdot \tanh(\text{MLP}(\Gamma_{PCA}(\mathbf{r}_i))), \end{aligned} \quad (7)$$

where  $\Gamma_{PCA}$  is the relative PCA model and  $M$  is the selected amount of linear basis. The MLP has three hidden layers with 256 neurons each and ReLU activations. We use a scaled tanh activation function for the output, to restrict the prediction to be in  $[-3\sigma, 3\sigma]$ . The final 3D model is obtained by  $\hat{\mathbf{S}} + \mathbf{p}_i^T \hat{\mathbf{S}}$  which is splatted using 3DGS. We follow the objective function from Equation 4 for supervision on the color reproduction with an additional L1 regularization w.r.t. the corresponding coefficients. We use AdamW with a learning rate  $1e-3$  and train it for 200k iterations with batch size one on a single Nvidia Quadro A6000 which takes around 4h.

## 5 Results

We evaluate our appearance model against state-of-the-art methods on the NeRSemble [33] dataset. We use the tracked meshes provided by Qian et al. [53] and the synchronized images from 16 cameras with a resolution of  $802 \times 550$ . Our main baselines are Gaussian Avatars (**GA**) [53] which is neural network-free (Gaussians are attached to the FLAME model), our implementation of Animatable Gaussians (**AG**) [38] which is based on CNN-predicting Gaussian maps, and INSTA [84] which uses dynamic NeRF [43]. For the comparison, we present

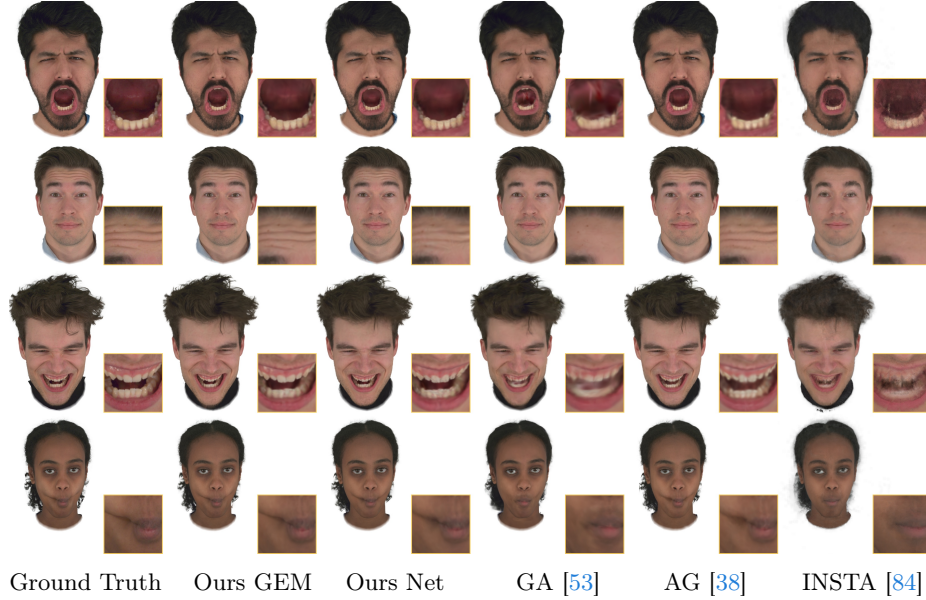


**Fig. 5: Novel view synthesis.** Both, the network and GEM, show better performance on novel views, especially, in the region of the mouth interior and wrinkles. In this experiment, we are following the evaluation of Gaussian Avatars [53] and demonstrate novel viewpoint generation. GEM is obtained throughout analysis-by-synthesis fitting [3, 67]. Note that the expressions are seen during training.

both of our appearance models, the StyleUNet-based architecture (**Ours Net**) and the distilled linear eigen model (**Ours GEM**) which we evaluate using analysis-by-synthesis fitting to the target images following [3, 67, 85]. Additionally, we show cross-reenactment results based on relative FLAME parameters transfer [84] as well as our coefficients regressor versus other baselines which are using FLAME meshes regressed by DECA [9] instead of the ground truth ones from [53]. All of the methods are evaluated using several image space metrics on novel expressions and novel views, following the test and novel-view split from Qian et al. [53]. For all of our experiments with eigenbasis, we use 50 components distilled from  $256^2$  textures which give around 60k active Gaussians. Animatable Gaussians [38] use a similar amount of primitives for front and back textures and Gaussian Avatars [53] typically use around 100k Gaussians.

### 5.1 Image Quality Evaluation

To evaluate our method, we measure the color error in the image space using the following metrics: PSNR (dB), LPIPS [77], L1 loss, and structural similarity

**Table 1:** Evaluation on novel expressions and views shows improved results of our GEM optimized using analysis-by-synthesis compared to others. See 6 for the corresponding qualitative results.

**Table 2:** Novel viewpoint evaluation on a withhold camera, corresponding to Figure 5. Note that the expressions have been seen during training, and only the view is new, the same as in GA [53].

Method	PSNR $\uparrow$	LPIPS $\downarrow$	SSIM $\uparrow$	L1 $\downarrow$	Method	PSNR $\uparrow$	LPIPS $\downarrow$	SSIM $\uparrow$	L1 $\downarrow$
Ours GEM	<b>32.6781</b>	<b>0.0675</b>	<b>0.9633</b>	<b>0.0069</b>	Ours GEM	<b>33.5528</b>	<b>0.0678</b>	<b>0.9662</b>	<b>0.0061</b>
Ours Net	29.2454	0.0777	0.9448	0.0096	Ours Net	32.4622	0.0713	0.9617	0.0067
AG [38]	29.0114	0.0812	0.9429	0.0099	AG [38]	32.4166	0.0712	0.9614	0.0066
GA [53]	28.3137	0.0815	0.9433	0.0102	GA [53]	31.3197	0.0786	0.9567	0.0075
INSTA [84]	27.9181	0.1153	0.9340	0.0128	INSTA [84]	27.7786	0.1232	0.9294	0.0163

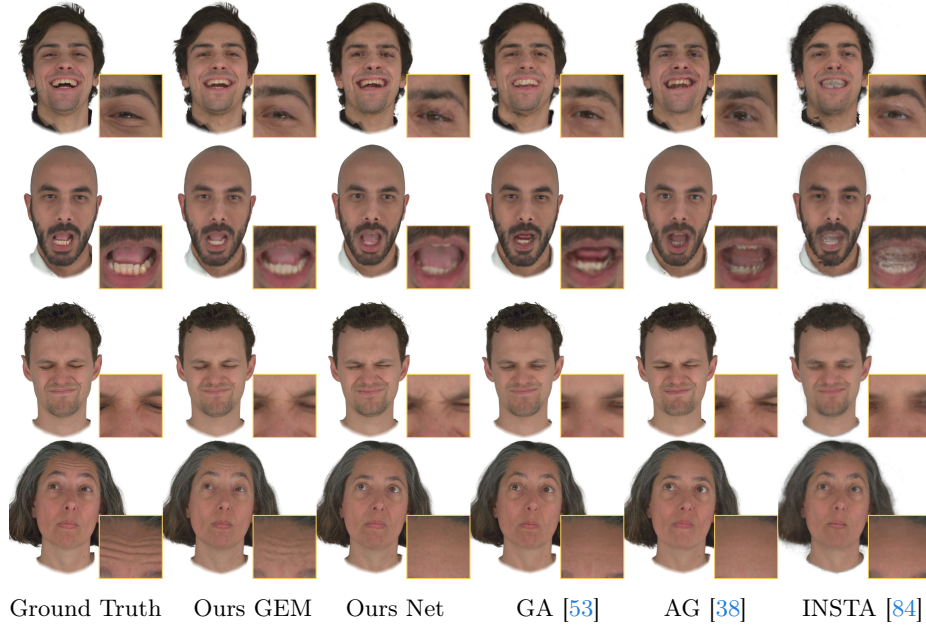
(SSIM). We follow the evaluation scheme from Gaussian Avatars [53], using their train and validation split. The evaluation of GEM was generated by sequentially fitting the coefficients to each image using the same objectives from Equation 4. Note that the baselines use the FLAME model with offsets for the tracking, while GEM can directly be used for modeling.

Table 1 presents results on novel expressions evaluated on all 16 cameras. Both the quantitative and qualitative results depicted in Figure 6 show that our PCA model produces fewer artifacts, especially for regions like teeth or facial wrinkles. Table 2 contains an evaluation where we measure errors on novel viewpoints. The results show that our CNN-based appearance model outperforms other neural methods, and, our linear eigenbasis GEM achieves the highest quality due to the ‘direct’ analysis-by-synthesis which can fully utilize the expressiveness and grade of our photo-realistic appearance model and is not restricted by 3DMMs like FLAME. Moreover, Figure 5 shows qualitative results of our method on novel views. As can be seen, we better capture high-frequency details, pose-dependent wrinkles, and self-shadows - something which is not possible for methods like Gaussian Avatars [53] or INSTA [84] since they either do not use pose-dependent neural networks or limit the conditioning to a small region only.

## 5.2 Cross-person Reenactment Evaluation

Facial cross-person reenactment transfers expressions from the source actor to the target actor. Most of the methods require tracked meshes obtained by fitting the FLAME model for each frame of the source actor sequence. From this tracking, the expression parameters are extracted and the relative change is applied to the neutral target face [67], see Figure 7. While this is an effective approach, it requires having the tracked mesh in a consistent mesh topology, which is a computationally intensive problem, especially in multi-view capture setups.

An alternative way is to use a (monocular) regressor like EMOCA [7] which, in real-time, can predict FLAME parameters for a single frame. We showcase this in comparison to our GEM which is driven by our image-based regressor, see Figure 8. As can be seen in both experiments, our network-based and GEM



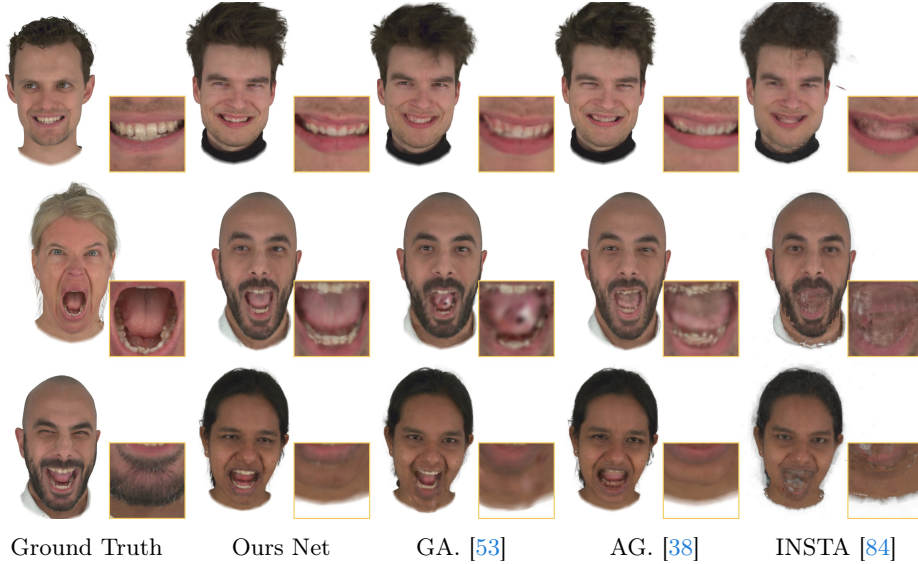
**Fig. 6: Novel view and expression synthesis.** Our Gaussian Eigen Model shows better results in regions like teeth, wrinkles, and self-shadows compared to other methods that struggle with artifacts.

can produce sharp results. The baseline methods have problems extrapolating to the new expressions, showing severe artifacts in the appearance. Our personalized approach effectively regularizes the regressed coefficients such that the predicted avatar stays in the training distribution effectively avoiding artifacts like in INSTA or Gaussian Avatars.

Drawing inspiration from EMOCA [7], we further assess cross-re-enactment quantitatively by leveraging emotion recognition feature vectors from both the source image and the resulting cross-re-enactment, utilizing EmoNet [68]. For each pair of input and output images, we predict EmoNet features and measure cosine distance and  $\mathcal{L}_1$  error between them. We report the numbers in the

**Table 3:** Cross-re-enactment evaluation employing EmoNet features and FID score. \*FPS omits the EMOCA forward pass time, which adds approximately 21 FPS to the inference.

Method	$\mathbf{E}_{feat} \cos \uparrow$	$\mathbf{E}_{feat} \mathcal{L}_1 \downarrow$	FID $\downarrow$	*FPS $\uparrow$
AG	0.9396	5.3399	0.4093	16.51
GA	0.8917	6.6141	0.5593	142.71
INSTA	0.9087	6.3153	0.5299	20.62
Ours Net	0.9440	5.1044	0.3685	35.77
Ours GEM	0.9381	5.3197	0.4286	201.70



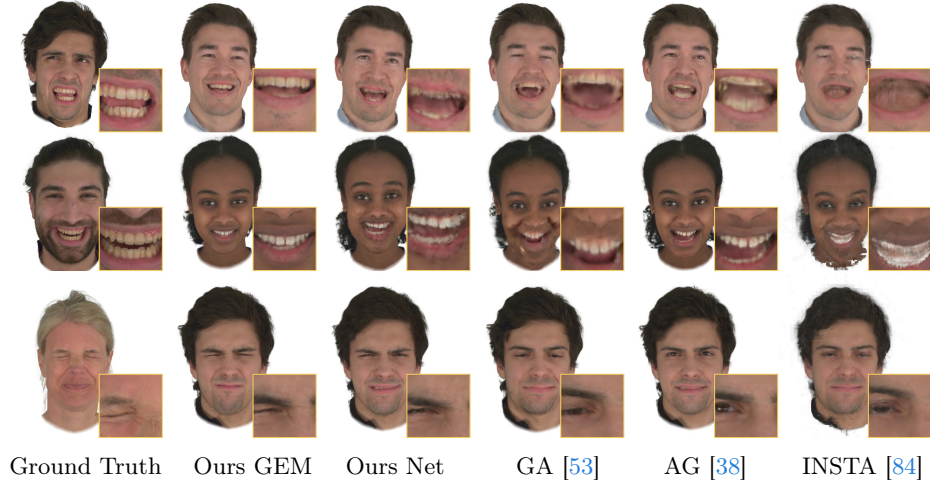
**Fig. 7: Facial cross-person reenactment.** The person’s expressions on the left are transferred to the respective avatars on the right. In this experiment, we are using relative expressions based on ground truth meshes from the dataset (FLAME-based meshes reconstructed from multi-view data). Note that this experiment does not apply to our GEM, since it is mesh-free.

Table 3. Additionally, we also report FID scores [19] and rendering speed. Our method achieves on-par quality with a CNN-based solution while maintaining the highest frame rates and significantly outperforming GA in terms of quality.

**Table 4: Ablation of GEM.** Even with 10 principle components a high PSNR of  $31.81dB$  is achieved, while taking only 7MB of memory. In contrast to fixed-sized neural networks, the GEM can be adjusted on the fly depending on the hardware. Moreover, since evaluation requires a single dot product for forward pass the rendering speed is around four times higher than our network. The speed evaluation was done using a single Nvidia A100 GPU.

#Comp	128 <sup>2</sup>			256 <sup>2</sup>			512 <sup>2</sup>		
	PSNR ↑	Size MB	FPS ↑	PSNR ↑	Size MB	FPS ↑	PSNR ↑	Size MB	FPS ↑
10	31.81	7	237.96	31.88	28	210.03	32.23	113	130.46
30	34.20	20	241.31	34.17	83	208.19	34.84	333	112.73
50	34.67	34	238.7	34.61	138	201.70	35.45	553	117.45
Ours Net	33.97	82	47.70	34.99	109	35.77	35.02	178	26.31
AG [38]	33.77	487	18.93	34.40	529	16.51	35.15	636	13.08





**Fig. 8: Facial cross-person reenactment using an image-based regressor.** The reenactment of the baselines is performed using relative transfer between FLAME meshes regressed by EMOCA compared to our GEM regressor network (Ours GEM).

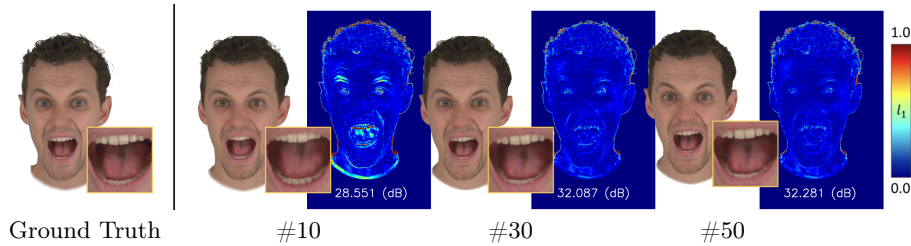


**Fig. 9: Compression error depending on the number of used eigenbasis components.** The heatmaps show the photometric  $\ell_1$ -error for 10, 30, and 50 components using  $128^2$  Gaussian maps. Full evaluation in the supp mat.

### 5.3 GEM Compression Ablation

In this section, we perform ablation of our linear GEM model in several aspects. First, we measure the memory size of such a model depending on the number of selected components compared to the size of the regressed texture. Secondly, we are interested in the compression error introduced by the projection on different amounts of principal components. Table 4 shows how the size in MB changes depending on the amount of basis and the source texture size. For instance, our smallest model weighs as little as **7MB** using only 10 components of the eigenbasis. This is almost **12** times less than our smallest CNN-based model and almost **70** times less than Animatable Gaussians [38]. In contrast to neural networks, we can easily trade quality over size which is very useful in the context of different commodity devices with reduced compute capabilities. Table 4 presents how compression affects the quality of reconstruction. We evaluated  $\sim 1k$  frames for



a single actor under a novel view. As expected using only 10 first components impacts the quality the most, however, the results are still high-quality as can be seen in Figure 9. As we previously discussed, to capture wrinkles and high-frequency details one needs to employ neural networks. Gaussian Avatars [53] offers a small size of the stored Gaussians cloud, ranging from 5MB, and 14MB without the FLAME model for  $128^2$ ,  $256^2$  Gaussians, respectively. However, the quality of reconstruction lacks wrinkle details and sharpness as can be seen in Figure 10. Note that our model does not require a FLAME model that weights an additional **90MB** compared to Gaussian Avatars [53]; Table 4 presents our absolute size values.

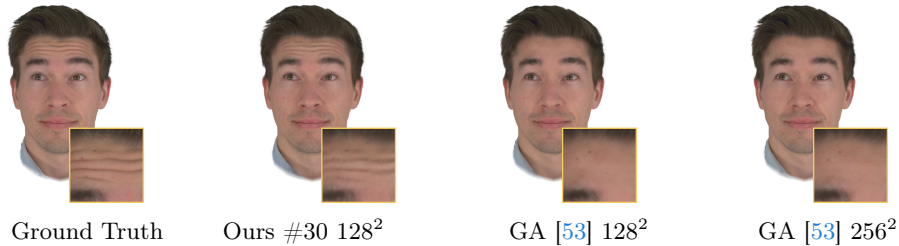


**Fig. 10:** The quality comparison to Gaussian Avatars [53] shows better performance even though our model is similar in size to its Gaussian cloud and we do **not** need an additional FLAME model which weighs 90MB.

#### 5.4 Universality of GEM

We designed GEM to be a universal method capable of distilling any 3DGS-based avatar solution [15, 28, 38, 53, 74] into a lightweight representation, as long as normalized input across training frames is provided. Our results show that a compact representation of the linear basis produces state-of-the-art results in terms of quality and speed. Figure 11 demonstrates how we can apply GEM to different primitive generators (AG [38], GA [53], Our Net). Note that to achieve wrinkle-level details, the generator itself has to produce high-quality output. As can be seen, we can apply our distillation technique to existing methods, making them light and compact. Moreover, GEM is well-suited for commodity devices, as it generates a new set of Gaussian primitives with only a single dot product needed between coefficients and the basis. We believe that this potential has great implications for downstream tasks such as holoportation, audio-driven avatars, or virtual reality.

## 6 Human Head Avatar Compression

Human avatar compression is an important topic, but it is still in its early stages and not well-explored. For neural-based representations, there are methods to compress networks, such as pruning [18], quantization [23], or knowledge distillation [20], as well as small and compact MobileNets [21]. Interestingly, in the

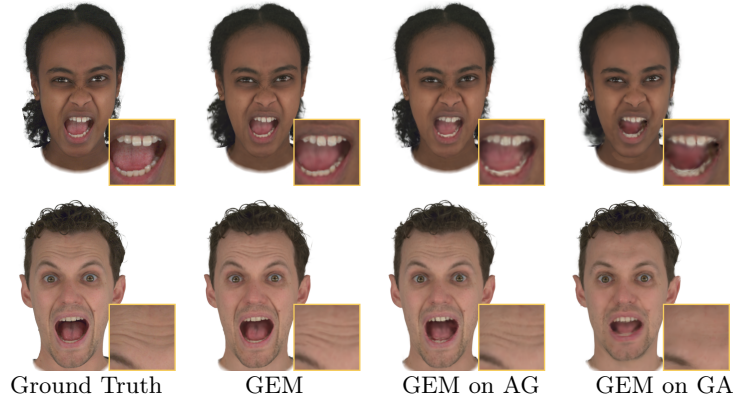


**Fig. 11:** GEM applied on different avatar methods (AG and GA) and optimized using analysis-by-synthesis. Our method is universal and can be successfully used on both; point clouds as well as textures to distill a lightweight avatar.

latter context, GEM can be considered as a single-layer MLP without any activation function. Unfortunately, these methods still require an expensive forward pass and may not be well-suited for all commodity devices.

The recently introduced Gaussian Avatars by Qian [53] also represents a form of avatar compression, though not in the primitives’ space but rather in the geometry space, with Gaussians attached and deformed by triangles from a linear face model. However, this form of appearance representation is insufficient for capturing details such as wrinkles, as it rigidly adheres to FLAME rigging in the geometry space. Therefore, we advocate for different compression techniques like GEM, which can leverage more powerful representations and distill them into expressive, high-quality linear models. We hope that this project will open doors to different methods for efficiently storing and representing avatars.

## 7 Discussion

Despite state-of-the-art results for human face avatars, our method has still certain limitations which we would like to discuss. One of the major drawbacks of the PCA-based models is their global extent. Which ultimately means that we cannot control local changes and produce more combinations of local features beyond the standard model. Thus, further work could include incorporating a localized PCA basis [44] for better avatar control, which could potentially enable a wider range of expressions outside the training set. Another limitation is the personalization, for new subjects a new representation has to be learned from multi-view data. An interesting future avenue would be to create a statistical model across different subjects.

## 8 Conclusion

We have proposed Gaussian Eigen Model, a linear appearance model that can represent photo-realistic facial avatars. The simplicity of this appearance model results in massively reduced compute requirements in comparison to CNN-based avatar methods. Moreover, the lightweight representation could improve the management, sharing, and applicability of avatars. The universal distillation approach can be applied to many existing methods, making them available for compression. We demonstrate how such a representation can be used in different scenarios like self-reenactment and cross-person animation. We also show that real-time applications are possible. We believe that the proposed GEM is a stepping stone toward lightweight avatar animation on consumer-level hardware.

# Gaussian Eigen Models for Human Heads

## –Supplemental Materials–

Wojciech Zielonka<sup>1</sup>, Timo Bolkart<sup>2</sup>, Thabo Beeler<sup>2</sup>, and Justus Thies<sup>1,3</sup>

<sup>1</sup>Max Planck Institute for Intelligent Systems, Tübingen, <sup>2</sup>Google, <sup>3</sup>TU Darmstadt  
<https://zielon.github.io/gem/>

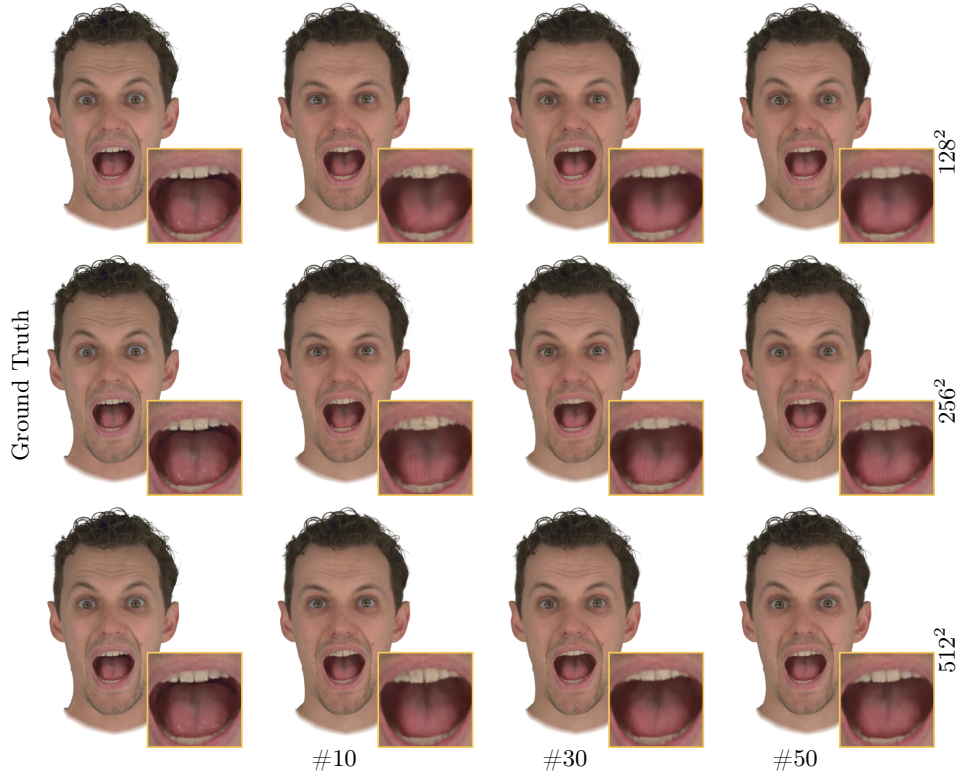


**Fig. 1:** Qualitative compression quality depending on the number of basis (10, 30, 50) and resolution of the Gaussian map (128<sup>2</sup>, 256<sup>2</sup>, 512<sup>2</sup>).

## 1 Compression Ablation Study

In the domain of 3D Morphable Models, principle component analysis (PCA) emerges as a cornerstone approach, instrumental in crafting the foundational framework for capturing face expressions and shapes with remarkable fidelity [3, 37]. This methodology has been adopted with notable success, not only in

modeling facial features but also in extrapolating the nuances of human bodies [41, 46, 49], and even in depicting intricate hand modeling [56].

Expanding upon this foundation, GEM proposes a novel technique involving an ensemble of eigenbasis of 3D Gaussian attributes for achieving a photorealistic human head appearance. This representation exhibits significant adaptability concerning both quality and size, leveraging a fundamental trait of linear basis that proves beneficial when applied to diverse devices with varying capabilities in digital human applications. Figures 1 and 2 illustrate the qualitative and quantitative results of GEM. Notably, even under substantial compression (utilizing only ten principal components), our approach consistently yields high-quality outcomes. More examples can be found in Figures (6, 4, 7, 5)

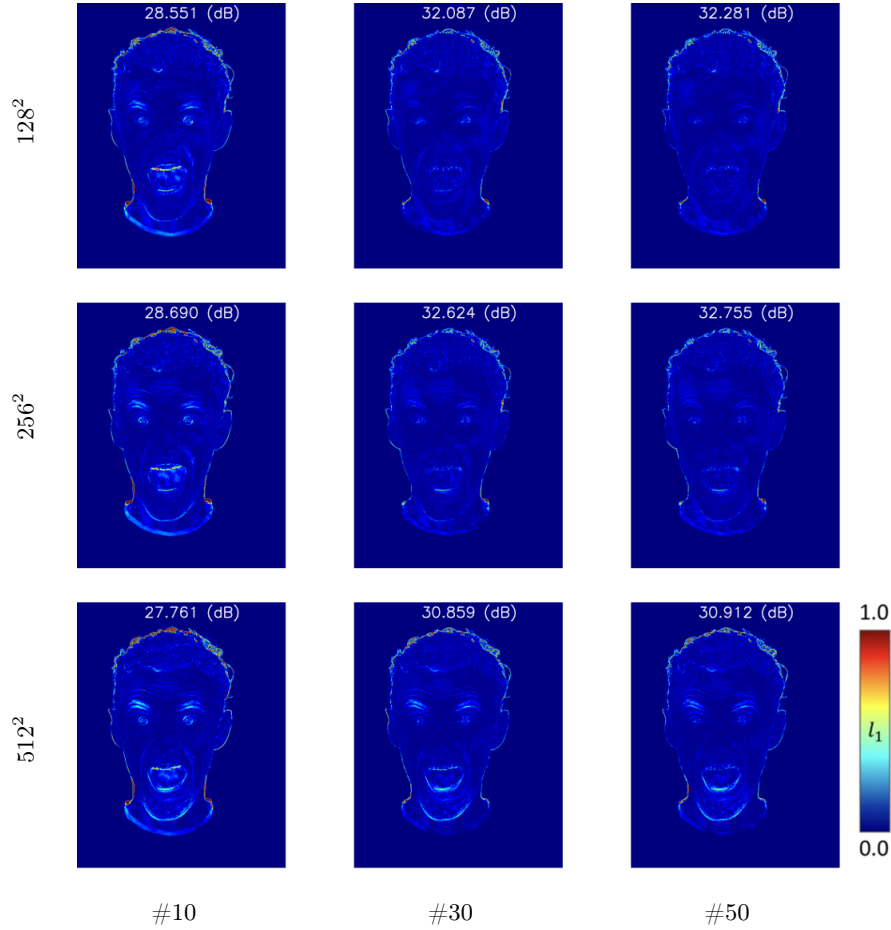


**Fig. 2:** Compression error in PSNR (db) depending on the number of basis (10, 30, 50) and resolution of the Gaussian maps ( $128^2$ ,  $256^2$ ,  $512^2$ ).

## 2 Additional Dataset Evaluation

In Figure 8, we provide further evaluation of our approach using the Multiface dataset [72]. This dataset encompasses short sequences of facial expressions, ranging from "relaxed mouth open" to "show all teeth" or "jaw open huge smile." The expressions vary widely in length and complexity, presenting a considerable challenge for analysis. It's important to note that this dataset does not provide a parametric 3DMM; instead, it offers meshes in full correspondence. However, as mentioned in the main text, our method remains adaptable in this context. By leveraging the deformation gradient [60] to transform points from canonical space into deformed space, and assuming consistent UV parametrization of input meshes, we can successfully navigate between these spaces. As depicted in Figure 8, our network demonstrates the ability to extrapolate to novel expressions, even amidst highly challenging facial poses.

## 3 Broader Impact

Our project focuses on reconstructing a highly detailed human face avatar from multiview videos, enabling the extrapolation of expressions not originally captured. While our technology serves primarily constructive purposes, such as enriching telepresence or mixed reality applications, we acknowledge the potential risks of misuse. Therefore, we advocate for advancements in digital media forensics [57, 58] to aid in detecting synthetic media. Additionally, we emphasize the importance of conducting research in this area with transparency and openness, including the thorough disclosure of algorithmic methodologies, data origins, and models intended for research purposes.

## 4 Future Applications & Discussion

An interesting application venue for GEM would be a combination of audio-driven methods with the appearance offered by our methods. Ng et al. [45] presented photorealistic audio-driven full-body avatars. Despite impressive results, the face region still does not fully convey expressions and lacks realism. One way of improving it would be incorporating recent progress in audio-driven geometry [2, 6, 65, 66] with a dedicated appearance model offered by GEM and our image-space regressor Figure 3.

Moreover, GEM neural network uses meshes to obtain normal maps as input to the Gaussian map regressor. However, meshes are limited by resolution and expressiveness, one way of improving on that would be to use NPHM by [13] by Giebenhain et al. and the follow-up work [14, 31, 61] to further increase the expressiveness of the model by explicitly capturing regions like hair or teeth.



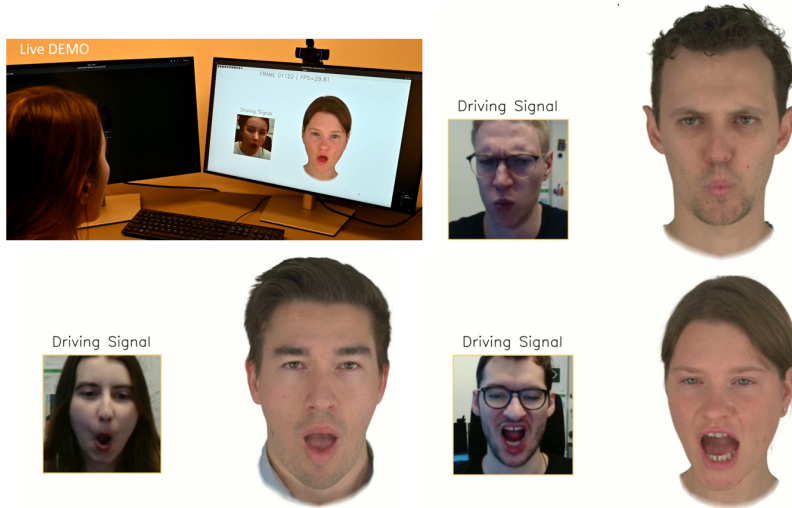


**Fig. 3:** GEM can be effectively controlled in real-time by an image-space regressor which produces coefficients projected on the linear basis of a personalized GEM avatar.



**Fig. 4:** Qualitative compression quality depending on the number of basis (10, 30, 50) and resolution of the Gaussian map ( $128^2$ ,  $256^2$ ,  $512^2$ ).

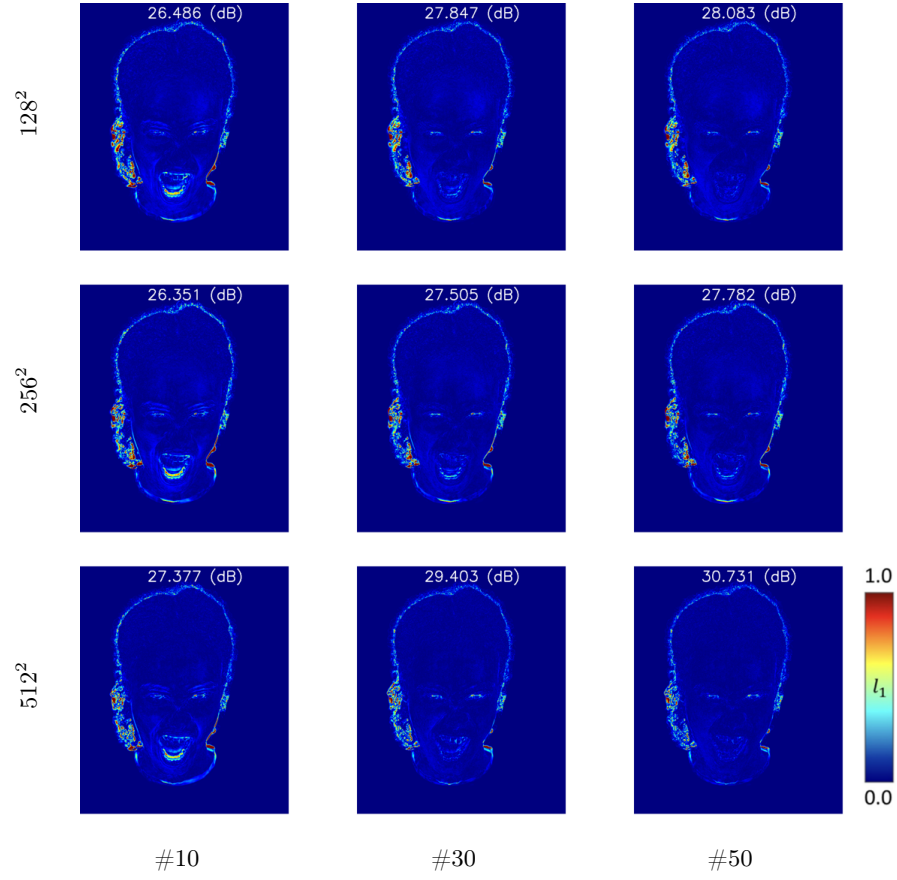


**Fig. 5:** Compression error in PSNR (db) depending on the number of basis (10, 30, 50) and resolution of the Gaussian maps ( $128^2$ ,  $256^2$ ,  $512^2$ ).

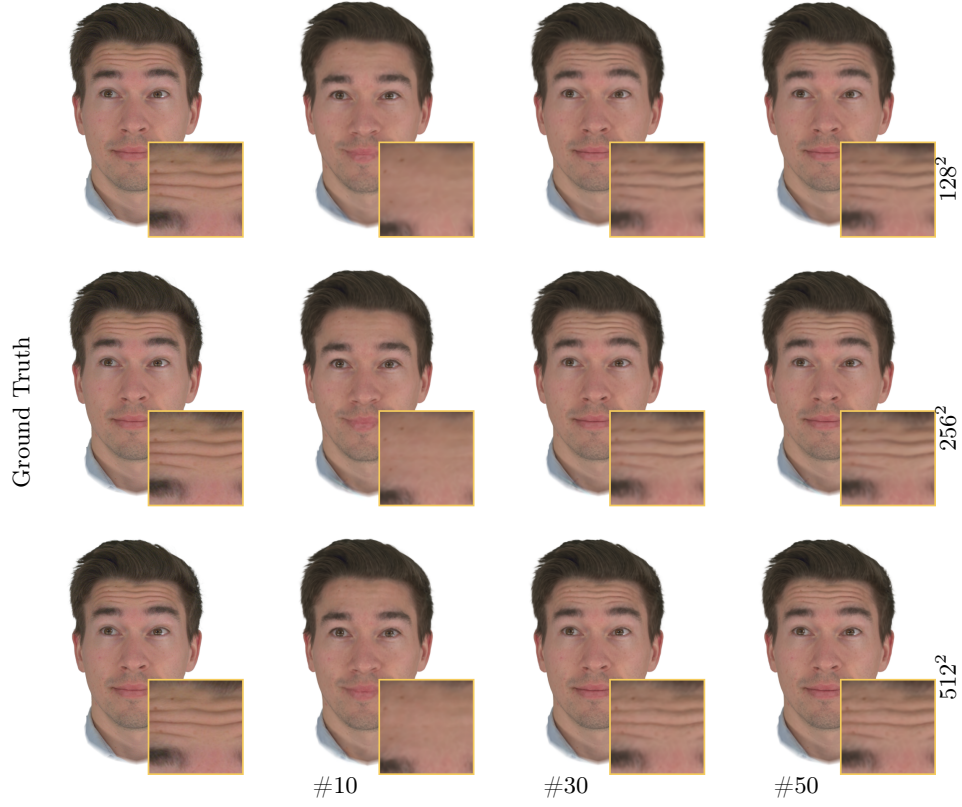


**Fig. 6:** Qualitative compression quality depending on the number of basis (10, 30, 50) and resolution of the Gaussian map ( $128^2$ ,  $256^2$ ,  $512^2$ ).

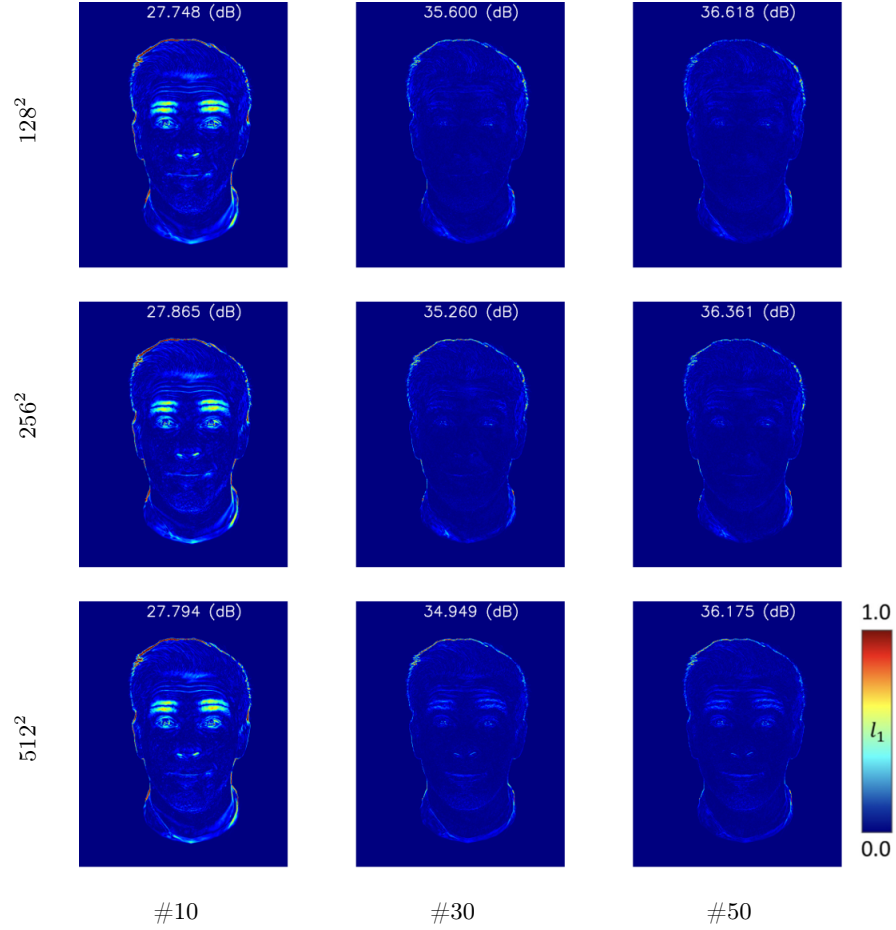


**Fig. 7:** Compression error in PSNR (db) depending on the number of basis (10, 30, 50) and resolution of the Gaussian maps ( $128^2$ ,  $256^2$ ,  $512^2$ ).



Ground Truth Ours Net Ours GEM Ground Truth Ours Net Ours GEM

**Fig. 8:** The Multiface dataset, introduced by Wu et al. [72], comprises actors performing scripted expressions in short segments. A notable challenge arises due to the occurrence of several expressions, like "show all teeth," appearing only once in the dataset. This poses a difficulty during testing, particularly when the network is required to extrapolate. Here we showcase the outcomes of the test sequences to illustrate the effectiveness of our CNN-based network in capturing diverse and challenging facial poses, demonstrating its robustness despite the inherent complexity of the dataset.



Ground Truth Ours GEM AG [38] GA [53] PointAvatar [82] AvatarMAV [75]

**Fig. 9:** Additional baselines PointAvatar (PSNR: 25.8, SSIM: 0.893 LPIPS: 0.097) and AvatarMAV (PSNR: 29.5, SSIM: 0.913, LPIPS: 0.152) evaluated on the novel-view sequences.

## References

1. An, S., Xu, H., Shi, Y., Song, G., Ogras, U.Y., Luo, L.: PanoHead: Geometry-aware 3D full-head synthesis in 360°. *Conference on Computer Vision and Pattern Recognition (CVPR)* pp. 20950–20959 (2023) [3](#)
2. Aneja, S., Thies, J., Dai, A., Nießner, M.: Facetalk: Audio-driven motion diffusion for neural parametric head models. *Conference on Computer Vision and Pattern Recognition (CVPR)* (2024) [20](#)
3. Blanz, V., Vetter, T.: A morphable model for the synthesis of 3D faces. In: *SIGGRAPH*. pp. 187–194 (1999) [2](#), [3](#), [10](#), [18](#)
4. Cao, C., Simon, T., Kim, J.K., Schwartz, G., Zollhoefer, M., Saito, S., Lombardi, S., Wei, S.E., Belko, D., Yu, S.I., Sheikh, Y., Saragih, J.M.: Authentic volumetric avatars from a phone scan. *Transactions on Graphics (TOG)* **41**, 1 – 19 (2022) [4](#)
5. Chan, E., Lin, C.Z., Chan, M., Nagano, K., Pan, B., Mello, S.D., Gallo, O., Guibas, L.J., Tremblay, J., Khamis, S., Karras, T., Wetzstein, G.: Efficient geometry-aware 3D generative adversarial networks. *Conference on Computer Vision and Pattern Recognition (CVPR)* pp. 16102–16112 (2021) [3](#)
6. Cudeiro, D., Bolkart, T., Laidlaw, C., Ranjan, A., Black, M.: Capture, learning, and synthesis of 3D speaking styles. In: *Proceedings IEEE Conf. on Computer Vision and Pattern Recognition (CVPR)*. pp. 10101–10111 (2019) [20](#)
7. Danecek, R., Black, M.J., Bolkart, T.: EMOCA: Emotion driven monocular face capture and animation. In: *Conference on Computer Vision and Pattern Recognition (CVPR)*. pp. 20311–20322 (2022) [8](#), [9](#), [11](#), [12](#)
8. Egger, B., Smith, W.A.P., Tewari, A., Wuhler, S., Zollhoefer, M., Beeler, T., Bernard, F., Bolkart, T., Kortylewski, A., Romdhani, S., Theobalt, C., Blanz, V., Vetter, T.: 3D morphable face models—past, present, and future. *Transactions on Graphics (TOG)* **39**(5) (2020) [2](#), [3](#)
9. Feng, Y., Feng, H., Black, M.J., Bolkart, T.: Learning an animatable detailed 3D face model from in-the-wild images. *Transactions on Graphics (TOG)* **40**, 1 – 13 (2020) [2](#), [8](#), [10](#)
10. Feng, Y., Feng, X., Shang, Y., Jiang, Y., Yu, C., Zong, Z., Shao, T., Wu, H., Zhou, K., Jiang, C., Yang, Y.: Gaussian splashing: Dynamic fluid synthesis with gaussian splatting (2024) [4](#)
11. Gafni, G., Thies, J., Zollhofer, M., Nießner, M.: Dynamic neural radiance fields for monocular 4D facial avatar reconstruction. *Conference on Computer Vision and Pattern Recognition (CVPR)* pp. 8645–8654 (2020) [2](#), [3](#), [4](#)
12. Gao, X., Zhong, C., Xiang, J., Hong, Y., Guo, Y., Zhang, J.: Reconstructing personalized semantic facial nerf models from monocular video. *Transactions on Graphics (TOG)* **41**, 1 – 12 (2022) [3](#)
13. Giebenhain, S., Kirschstein, T., Georgopoulos, M., Rünz, M., Agapito, L., Nießner, M.: Learning neural parametric head models. In: *Proc. IEEE Conf. on Computer Vision and Pattern Recognition (CVPR)* (2023) [20](#)
14. Giebenhain, S., Kirschstein, T., Georgopoulos, M., Rünz, M., Agapito, L., Nießner, M.: Mononphm: Dynamic head reconstruction from monocular videos. In: *Proc. IEEE Conf. on Computer Vision and Pattern Recognition (CVPR)* (2024) [20](#)
15. Giebenhain, S., Kirschstein, T., Rünz, M., Agapito, L., Nießner, M.: Npga: Neural parametric gaussian avatars (2024), <https://arxiv.org/abs/2405.19331> [4](#), [15](#)
16. Goral, C.M., Torrance, K.E., Greenberg, D.P., Battaile, B.: Modeling the interaction of light between diffuse surfaces. *SIGGRAPH* (1984) [5](#)



17. Grassal, P., Prinzler, M., Leistner, T., Rother, C., Nießner, M., Thies, J.: Neural head avatars from monocular RGB videos. In: Conference on Computer Vision and Pattern Recognition (CVPR). pp. 18632–18643 (2022) [2](#), [3](#), [4](#), [8](#)
18. Han, S., Pool, J., Tran, J., Dally, W.J.: Learning both weights and connections for efficient neural networks (2015), <https://arxiv.org/abs/1506.02626> [15](#)
19. Heusel, M., Ramsauer, H., Unterthiner, T., Nessler, B., Hochreiter, S.: Gans trained by a two time-scale update rule converge to a local nash equilibrium (2018), <https://arxiv.org/abs/1706.08500> [13](#)
20. Hinton, G., Vinyals, O., Dean, J.: Distilling the knowledge in a neural network (2015), <https://arxiv.org/abs/1503.02531> [15](#)
21. Howard, A.G., Zhu, M., Chen, B., Kalenichenko, D., Wang, W., Weyand, T., Andreetto, M., Adam, H.: Mobilenets: Efficient convolutional neural networks for mobile vision applications (2017), <https://arxiv.org/abs/1704.04861> [15](#)
22. Isola, P., Zhu, J.Y., Zhou, T., Efros, A.A.: Image-to-image translation with conditional adversarial networks (2018), <https://arxiv.org/abs/1611.07004> [5](#)
23. Jacob, B., Kligys, S., Chen, B., Zhu, M., Tang, M., Howard, A., Adam, H., Kalenichenko, D.: Quantization and training of neural networks for efficient integer-arithmetic-only inference (2017), <https://arxiv.org/abs/1712.05877> [15](#)
24. Jiang, Y., Yu, C., Xie, T., Li, X., Feng, Y., Wang, H., Li, M., Lau, H., Gao, F., Yang, Y., Jiang, C.: VR-GS: A physical dynamics-aware interactive gaussian splatting system in virtual reality (2024) [4](#)
25. Jolliffe, I.T.: Principal component analysis and factor analysis (1986) [8](#)
26. Kabadayi, B., Zielonka, W., Bhatnagar, B.L., Pons-Moll, G., Thies, J.: GAN-Avatar: Controllable personalized gan-based human head avatar. *ArXiv abs/2311.13655* (2023) [3](#)
27. Karras, T., Laine, S., Aittala, M., Hellsten, J., Lehtinen, J., Aila, T.: Analyzing and improving the image quality of StyleGAN. *IEEE/CVF Conference on Computer Vision and Pattern Recognition (CVPR)* pp. 8107–8116 (2019) [3](#), [5](#), [6](#)
28. Kerbl, B., Kopanas, G., Leimkuehler, T., Drettakis, G.: 3D gaussian splatting for real-time radiance field rendering. *Transactions on Graphics (TOG)* **42**, 1 – 14 (2023) [2](#), [3](#), [4](#), [5](#), [6](#), [15](#)
29. Kingma, D.P., Ba, J.: Adam: A method for stochastic optimization. *CoRR abs/1412.6980* (2014) [7](#)
30. Kingma, D.P., Welling, M.: Auto-encoding variational bayes (2022) [3](#)
31. Kirschstein, T., Giebenhain, S., Nießner, M.: Diffusionavatars: Deferred diffusion for high-fidelity 3d head avatars. *arXiv preprint arXiv:2311.18635* (2023) [20](#)
32. Kirschstein, T., Giebenhain, S., Tang, J., Georgopoulos, M., Nießner, M.: Gghead: Fast and generalizable 3d gaussian heads (2024), <https://arxiv.org/abs/2406.09377> [4](#)
33. Kirschstein, T., Qian, S., Giebenhain, S., Walter, T., Nießner, M.: NeRSemble: Multi-view radiance field reconstruction of human heads. *Transactions on Graphics (TOG)* **42**, 1 – 14 (2023) [7](#), [9](#)
34. Kopanas, G., Philip, J., Leimkuehler, T., Drettakis, G.: Point-based neural rendering with per-view optimization. *Computer Graphics Forum (CGF)* **40** (2021) [5](#)
35. Lassner, C., Zollhöfer, M.: Pulsar: Efficient sphere-based neural rendering. *Conference on Computer Vision and Pattern Recognition (CVPR)* pp. 1440–1449 (2021) [4](#)
36. Li, J., Saito, S., Simon, T., Lombardi, S., Li, H., Saragih, J.M.: MEGANE: Morphable eyeglass and avatar network. *Conference on Computer Vision and Pattern Recognition (CVPR)* pp. 12769–12779 (2023) [4](#)

37. Li, T., Bolkart, T., Black, M.J., Li, H., Romero, J.: Learning a model of facial shape and expression from 4D scans. *Transactions on Graphics, (Proc. SIGGRAPH Asia)* **36**(6), 194:1–194:17 (2017) [3](#), [4](#), [7](#), [18](#)
38. Li, Z., Zheng, Z., Wang, L., Liu, Y.: Animatable gaussians: Learning pose-dependent gaussian maps for high-fidelity human avatar modeling. *ArXiv abs/2311.16096* (2023) [2](#), [4](#), [5](#), [6](#), [9](#), [10](#), [11](#), [12](#), [13](#), [14](#), [15](#), [25](#)
39. Lombardi, S., Simon, T., Saragih, J.M., Schwartz, G., Lehrmann, A.M., Sheikh, Y.: Neural volumes. *Transactions on Graphics (TOG)* **38**, 1 – 14 (2019) [3](#), [4](#)
40. Lombardi, S., Simon, T., Schwartz, G., Zollhoefer, M., Sheikh, Y., Saragih, J.M.: Mixture of volumetric primitives for efficient neural rendering. *Transactions on Graphics (TOG)* **40**, 1 – 13 (2021) [4](#)
41. Loper, M., Mahmood, N., Romero, J., Pons-Moll, G., Black, M.J.: Smpl: A skinned multi-person linear model. *Seminal Graphics Papers: Pushing the Boundaries, Volume 2* (2023) [19](#)
42. Ma, S., Simon, T., Saragih, J., Wang, D., Li, Y., Torre, F.D.L., Sheikh, Y.: Pixel codec avatars (2021) [8](#)
43. Mildenhall, B., Srinivasan, P.P., Tancik, M., Barron, J.T., Ramamoorthi, R., Ng, R.: NeRF: Representing scenes as neural radiance fields for view synthesis. In: *European Conference on Computer Vision (ECCV)*. vol. 12346, pp. 405–421 (2020) [3](#), [4](#), [5](#), [9](#)
44. Neumann, T., Varanasi, K., Wenger, S., Wacker, M., Magnor, M.A., Theobalt, C.: Sparse localized deformation components. *ACM Transactions on Graphics (TOG)* **32**, 1 – 10 (2013) [16](#)
45. Ng, E., Romero, J., Bagautdinov, T., Bai, S., Darrell, T., Kanazawa, A., Richard, A.: From audio to photoreal embodiment: Synthesizing humans in conversations. *Conference on Computer Vision and Pattern Recognition (CVPR)* (2024) [20](#)
46. Osman, A.A.A., Bolkart, T., Tzionas, D., Black, M.J.: SUPR: A sparse unified part-based human body model. In: *European Conference on Computer Vision (ECCV)* (2022) [19](#)
47. Pang, H., Zhu, H., Kortylewski, A., Theobalt, C., Habermann, M.: ASH: Animatable gaussian splats for efficient and photoreal human rendering. *ArXiv abs/2312.05941* (2023) [2](#), [4](#), [5](#), [6](#)
48. Parke, F.I.: Computer generated animation of faces. In: *Proceedings of the ACM Annual Conference - Volume 1*. p. 451–457. ACM '72, Association for Computing Machinery, New York, NY, USA (1972) [2](#)
49. Pavlakos, G., Choutas, V., Ghorbani, N., Bolkart, T., Osman, A.A.A., Tzionas, D., Black, M.J.: Expressive body capture: 3D hands, face, and body from a single image. In: *Proceedings IEEE Conf. on Computer Vision and Pattern Recognition (CVPR)*. pp. 10975–10985 (2019) [19](#)
50. Paysan, P., Knothe, R., Amberg, B., Romdhani, S., Vetter, T.: A 3D face model for pose and illumination invariant face recognition. *IEEE International Conference on Advanced Video and Signal based Surveillance (AVSS)* (2009) [4](#)
51. Pedregosa, F., Varoquaux, G., Gramfort, A., Michel, V., Thirion, B., Grisel, O., Blondel, M., Louppe, G., Prettenhofer, P., Weiss, R., Weiss, R.J., Vanderplas, J., Passos, A., Cournapeau, D., Brucher, M., Perrot, M., Duchesnay, E.: Scikit-learn: Machine learning in python. *ArXiv abs/1201.0490* (2011) [8](#)
52. Prinzler, M., Hilliges, O., Thies, J.: DINER: Depth-aware Image-based NEural Radiance fields. *Conference on Computer Vision and Pattern Recognition (CVPR)* pp. 12449–12459 (2022) [3](#)

53. Qian, S., Kirschstein, T., Schoneveld, L., Davoli, D., Giebenhain, S., Nießner, M.: GaussianAvatars: Photorealistic head avatars with rigged 3D gaussians. ArXiv **abs/2312.02069** (2023) [2](#), [4](#), [7](#), [9](#), [10](#), [11](#), [12](#), [13](#), [14](#), [15](#), [16](#), [25](#)
54. Ramamoorthi, R., Hanrahan, P.: An efficient representation for irradiance environment maps. SIGGRAPH (2001) [5](#)
55. Remelli, E., Bagautdinov, T.M., Saito, S., Wu, C., Simon, T., Wei, S.E., Guo, K., Cao, Z., Prada, F., Saragih, J.M., Sheikh, Y.: Drivable volumetric avatars using texel-aligned features. SIGGRAPH (2022) [4](#)
56. Romero, J., Tzionas, D., Black, M.J.: Embodied hands: Modeling and capturing hands and bodies together. ACM Transactions on Graphics, (Proc. SIGGRAPH Asia) **36**(6) (Nov 2017) [19](#)
57. Rössler, A., Cozzolino, D., Verdoliva, L., Riess, C., Thies, J., Nießner, M.: Face-forensics: A large-scale video dataset for forgery detection in human faces. ArXiv (2018) [20](#)
58. Rössler, A., Cozzolino, D., Verdoliva, L., Riess, C., Thies, J., Nießner, M.: Face-forensics++: Learning to detect manipulated facial images. 2019 IEEE/CVF International Conference on Computer Vision (ICCV) pp. 1–11 (2019) [20](#)
59. Saito, S., Schwartz, G., Simon, T., Li, J., Nam, G.: Relightable gaussian codec avatars. ArXiv **abs/2312.03704** (2023) [2](#), [4](#)
60. Sumner, R.W., Popović, J.: Deformation transfer for triangle meshes. ACM SIGGRAPH (2004) [6](#), [20](#)
61. Tang, J., Dai, A., Nie, Y., Markhasin, L., Thies, J., Niessner, M.: Dphms: Diffusion parametric head models for depth-based tracking (2024) [20](#)
62. Teotia, K., MallikarjunB., R., Pan, X., Kim, H.J., Garrido, P., Elgharib, M.A., Theobalt, C.: HQ3DAvatar: High quality controllable 3D head avatar. ArXiv **abs/2303.14471** (2023) [4](#)
63. Tewari, A., Fried, O., Thies, J., Sitzmann, V., Lombardi, S., Sunkavalli, K., Martin-Brualla, R., Simon, T., Saragih, J., Nießner, M., Pandey, R., Fanello, S., Wetzstein, G., Zhu, J.Y., Theobalt, C., Agrawala, M., Shechtman, E., Goldman, D.B., Zollhöfer, M.: State of the art on neural rendering. EG (2020) [2](#), [3](#)
64. Tewari, A., Thies, J., Mildenhall, B., Srinivasan, P., Treischk, E., Wang, Y., Lassner, C., Sitzmann, V., Martin-Brualla, R., Lombardi, S., Simon, T., Theobalt, C., Niessner, M., Barron, J.T., Wetzstein, G., Zollhoefer, M., Golyanik, V.: Advances in neural rendering (2022) [2](#), [3](#)
65. Thambiraja, B., Aliakbarian, S., Cosker, D., Thies, J.: 3DiFACE: Diffusion-based speech-driven 3D facial animation and editing. ArXiv **abs/2312.00870** (2023) [20](#)
66. Thambiraja, B., Habibie, I., Aliakbarian, S., Cosker, D.P., Theobalt, C., Thies, J.: Imitator: Personalized speech-driven 3D facial animation. International Conference on Computer Vision (ICCV) pp. 20564–20574 (2022) [20](#)
67. Thies, J., Zollhöfer, M., Stamminger, M., Theobalt, C., Nießner, M.: Face2Face: Real-time face capture and reenactment of RGB videos. Conference on Computer Vision and Pattern Recognition (CVPR) pp. 2387–2395 (2016) [3](#), [8](#), [9](#), [10](#), [11](#)
68. Toisoul, A., Kossaifi, J., Bulat, A., Tzimiropoulos, G., Pantic, M.: Estimation of continuous valence and arousal levels from faces in naturalistic conditions. Nature Machine Intelligence (2021), <https://www.nature.com/articles/s42256-020-00280-0> [12](#)
69. Wang, L., Zhao, X., Sun, J., Zhang, Y., Zhang, H., Yu, T., Liu, Y.: StyleAvatar: Real-time photo-realistic portrait avatar from a single video. In: SIGGRAPH. pp. 67:1–67:10 (2023) [2](#), [3](#), [4](#), [5](#), [6](#)

70. Wang, Y., Serena, F., Wu, S., Öztireli, C., Sorkine-Hornung, O.: Differentiable surface splatting for point-based geometry processing. *Transactions on Graphics (TOG)* **38**, 1 – 14 (2019) [4](#), [5](#)
71. Wang, Z., Shen, T., Nimier-David, M., Sharp, N., Gao, J., Keller, A., Fidler, S., Müller, T., Gojcic, Z.: Adaptive shells for efficient neural radiance field rendering. *Transactions on Graphics (TOG)* **42**(6) (2023) [4](#)
72. Wu, C.h., Zheng, N., Ardisson, S., Bali, R., Belko, D., Brockmeyer, E., Evans, L., Godisart, T., Ha, H., Huang, X., Hypes, A., Koska, T., Krenn, S., Lombardi, S., Luo, X., McPhail, K., Millerschoen, L., Perdoch, M., Pitts, M., Richard, A., Saragih, J., Saragih, J., Shiratori, T., Simon, T., Stewart, M., Trimble, A., Weng, X., Whitewolf, D., Wu, C., Yu, S.I., Sheikh, Y.: Multiface: A dataset for neural face rendering. In: *arXiv* (2022) [20](#), [25](#)
73. Xie, T., Zong, Z., Qiu, Y., Li, X., Feng, Y., Yang, Y., Jiang, C.: PhysGaussian: Physics-integrated 3D gaussians for generative dynamics (2023) [4](#)
74. Xu, Y., Chen, B., Li, Z., Zhang, H., Wang, L., Zheng, Z., Liu, Y.: Gaussian head avatar: Ultra high-fidelity head avatar via dynamic gaussians. *ArXiv abs/2312.03029* (2023) [2](#), [4](#), [5](#), [15](#)
75. Xu, Y., Wang, L., Zhao, X., Zhang, H., Liu, Y.: Avatarmav: Fast 3d head avatar reconstruction using motion-aware neural voxels. In: *ACM SIGGRAPH 2023 Conference Proceedings* (2023) [25](#)
76. Xu, Y., Zhang, H., Wang, L., Zhao, X., Han, H., Guojun, Q., Liu, Y.: LatentAvatar: Learning latent expression code for expressive neural head avatar. In: *SIGGRAPH* (2023) [3](#)
77. Zhang, R., Isola, P., Efros, A.A., Shechtman, E., Wang, O.: The unreasonable effectiveness of deep features as a perceptual metric (2018) [10](#)
78. Zhao, X., Wang, L., Sun, J., Zhang, H., Suo, J., Liu, Y.: Havatar: High-fidelity head avatar via facial model conditioned neural radiance field. *Transactions on Graphics (TOG)* (2023) [3](#)
79. Zheng, S., Zhou, B., Shao, R., Liu, B., Zhang, S., Nie, L., Liu, Y.: GPS-gaussian: Generalizable pixel-wise 3D gaussian splatting for real-time human novel view synthesis. *ArXiv abs/2312.02155* (2023) [2](#)
80. Zheng, S., Zhou, B., Shao, R., Liu, B., Zhang, S., Nie, L., Liu, Y.: GPS-Gaussian: Generalizable pixel-wise 3d gaussian splatting for real-time human novel view synthesis. *arXiv* (2023) [4](#)
81. Zheng, Y., Abrevaya, V.F., Chen, X., Buhler, M.C., Black, M.J., Hilliges, O.: I M Avatar: Implicit morphable head avatars from videos. *Conference on Computer Vision and Pattern Recognition (CVPR)* pp. 13535–13545 (2021) [2](#), [3](#)
82. Zheng, Y., Wang, Y., Wetzstein, G., Black, M.J., Hilliges, O.: PointAvatar: Deformable point-based head avatars from videos. *Conference on Computer Vision and Pattern Recognition (CVPR)* pp. 21057–21067 (2022) [3](#), [25](#)
83. Zielonka, W., Bagautdinov, T.M., Saito, S., Zollhofer, M., Thies, J., Romero, J.: Drivable 3D gaussian avatars. *ArXiv abs/2311.08581* (2023) [2](#), [4](#), [6](#)
84. Zielonka, W., Bolkart, T., Thies, J.: Instant volumetric head avatars. *Conference on Computer Vision and Pattern Recognition (CVPR)* pp. 4574–4584 (2022) [3](#), [4](#), [8](#), [9](#), [10](#), [11](#), [12](#), [13](#), [14](#)
85. Zielonka, W., Bolkart, T., Thies, J.: Towards metrical reconstruction of human faces. In: *European Conference on Computer Vision (ECCV)* (2022) [10](#)
86. Zollhöfer, M., Thies, J., Bradley, D., Garrido, P., Beeler, T., Pérez, P., Stamminger, M., Nießner, M., Theobalt, C.: State of the art on monocular 3d face reconstruction, tracking, and applications (2018) [2](#), [3](#)

87. Zwicker, M., Pfister, H.R., van Baar, J., Gross, M.H.: Surface splatting. SIGGRAPH (2001) [4](#), [5](#)